Nuclear hormone receptor regulation of *Caudal* mediates ventral nerve cord assembly in *C. elegans*.

Nathaniel Noblett,[1,2] Tony Roenspies,[1] Stephane Flibotte,[3] and Antonio Colavita[1,2]

[1]Neuroscience Program, Ottawa Hospital Research Institute, Ottawa, Canada
[2]Department of Cellular and Molecular Medicine, University of Ottawa, Ottawa, Canada
[3]UBC/LSI Bioinformatics Facility, University of British Columbia, Vancouver, Canada

Highlights

- PAL-1 is required for proper neuron cell body positioning in the ventral nerve cord (VNC) in newly hatched worms.
- An upstream promoter element controls the expression of pal-1 in DD and DA neurons.
- The nuclear hormone receptor SEX-1 is for required for proper neuron positioning in the VNC.
- SEX-1 regulates PAL-1 expression in DD and DA neurons.

Abstract

The regulatory network governed by CDX/*Caudal* family transcription factors plays critical roles in shaping embryonic neural development. In *C. elegans*, we found that proper expression of PAL-1, the *C. elegans Caudal* orthologue, is required for correct positioning of motor neuron cell bodies in the first larval stage ventral nerve cord (VNC). We identified an upstream regulatory region within the *pal-1* promoter that drives *pal-1* expression in a subset of DD and DA neuronal progenitors. We also show that SEX-1, a nuclear hormone receptor, is required for motor neuron positioning in the VNC. Loss of *sex-1* results in neuronal positioning defects similar to those observed in *pal-1* mutants. This is due to a requirement for SEX-1 in promoting *pal-1* expression in DD and DA neuronal progenitors during VNC assembly. Double mutant analysis further suggests that SEX-1 also has *pal-1*-independent functions. Together, these findings define a transcriptional hierarchy in which the SEX-1 nuclear hormone receptor regulates the tissue-specific activity of PAL-1 to promote proper motor neuron positioning in the VNC and highlight a conserved role for CDX/Caudal family proteins in central nerve cord formation.

Keywords

C. elegans, motor neuron positioning, ventral nerve cord, *Caudal*, PAL-1, SEX-1

Introduction

The coordination of signaling cascades and positional information through transcriptional networks is essential for axial extension during embryonic morphogenesis (Collinet and Lecuit, 2021. The *Caudal* family of homeodomain transcription factors, including CDX1/2/4 in mammals and their worm ortholog PAL-1, play critical roles in posterior patterning and axial extension by coordinating pathways involved in cell-fate determination, morphogenesis and regionalization (Edgar et al., 2001; van den Akker et al., 2002; Gilbert et al., 2020; Zhu and Lohnes, 2022). For CDX proteins this includes the regulation of neurulation during mammalian development, a process where the neuroectoderm folds and elongates to form the neural tube (Savory et al., 2011; Zhao et al., 2014). Neurulation is partly driven by convergent extension, a morphogenetic process characterized by coordinated cell-cell intercalations along the mediolateral axis and extension along the anterior-posterior axis. Mouse embryos with mutations in both CDX1 and CDX2 exhibit typical convergent extension defects, including a reduced length-to-width ratio of the neural tube, failure of extension, and a broadened midline of the neural plate (Savory et al., 2011). These defects lead to embryonic lethality and craniorachischisis, a severe neural tube defect (Savory et al., 2011).

CDX proteins function as a central hub for multiple signaling pathways that regulate neurulation (Wilson et al., 2003; Palmer et al., 2021; Zhao et al., 2022). This includes the direct induction of CDX1 by retinoic acid receptors (RARs) α1 and γ, two types of ligand dependent nuclear hormone receptors, as well as β-catenin, a key component of canonical WNT signaling (Houle et al., 2003; Zhao et al., 2014). During neurulation, CDX members have been linked to regulation of the Planar Cell Polarity (PCP) pathway, a key pathway involved in convergent extension (Savory et al., 2011). PCP components associated with CDX include Scribble and the transmembrane receptor PTK7 (Wehner et al., 2011; Hayes et al., 2013; Martinez et al., 2015). Both CHiP analysis and transfection assays suggest that CDX proteins directly regulate PTK7 expression (Savory et al., 2011).

In *C. elegans*, PAL-1 is involved in cell fate determination, regional identity, and morphogenesis. PAL-1 plays an early role in blastomere cell fate, including a key role in establishing the fate of descendants of the C and D blastomeres (producing primarily body-wall muscle, hypodermal cells, along with two neurons) and, along with the WNT effector POP-1 and the bZIP transcription factor SKN-1, E blastomere (producing intestinal cells) (Hunter and Kenyon, 1996; Maduro et al., 2005). Additionally, PAL-1 is involved in non-cell fate related functions, such as orienting epidermal seam-cell migration and alignment during development (Gilbert et al., 2020). Other defects, including delays in ventral enclosure, failed long range migration in MS cell descendants and abnormal cleavage axis in muscle cells suggest that additional functions of a *pal-1* network remain to be explored (Edgar et al., 2001).

At hatching, the ventral nerve cord (VNC) in *C. elegans*, is comprised of 22 embryonically born motor neurons, belonging to three sub-types (6 GABAergic inhibitory DD, 9 cholinergic excitatory DA, and 7 cholinergic excitatory DB), that innervate body wall muscle to control sinusoidal locomotion (Lu et al., 2022). Progenitors of these neurons are born on the left and right sides of the embryo and undergo collective cell movement toward the midline where they intercalate to form the VNC. This process shares several core features with neurulation in mammals, including rosette mediated-convergent extension, asymmetric distribution of core PCP

components like VANG-1/VangL, and inositol phosphate signaling (Shah et al., 2017; Noblett et al., 2024).

Here, we describe roles for the nuclear hormone receptor SEX-1 and the *Caudal* homolog PAL-1 in regulating proper neuronal organization of the VNC. Using an allele that causes tissue-specific changes in gene expression, we identified a role for *pal-1* in regulating the proper positioning of embryonically derived motor neurons in the VNC. This region drives *pal-1* expression in a subset of neuronal progenitors during the stage of embryonic convergent extension movements that form the VNC. We found that SEX-1 is required for *pal-1* expression in progenitor neurons, and that restoring *pal-1* expression in these cells is sufficient to partially rescue the neuronal positioning defects in *sex-1* mutants. These findings reveal that nuclear hormone regulation of *Caudal* is important for VNC assembly highlight conserved mechanisms in central cord formation.

Results

Identification of a genomic region involved in the tissue specific regulation of *pal-1*.

The VNC at the first larval (L1) stage contains three classes of motor neurons (6 DD, 9 DA, and 7 DB). We have previously shown that loss of PCP genes, such as *vang-1*, and the Robo encoding gene *sax-3* result in VNC assembly defects during embryogenesis, which manifest as mispositioned motor neurons in L1 larvae (Shah et al., 2017). To identify new genes involved in neuron positioning, we performed a genetic screen using the DD-specific reporter *ynIs37[flp-13p::GFP]* (unpublished results). We identified two mutants, *zy43* and *zy44*, that displayed similar DD neuron positioning defects, with DD2 and DD3 positioned closer together than in wild type (WT) (Fig. 1A). Whole genome sequencing revealed these mutations to be single nucleotide changes, one nucleotide apart, located 143 and 145 bp upstream of the *arl-6* start codon (Fig. 1C). To determine if these changes were responsible for the neuron position defects, we used Cas9-targetted non-homologous end joining-mediated DNA repair to generate a 44 bp deletion (*zy117*) centered on the mutated region (Fig. 1C and D). This mutant displayed similar neuron positioning defects (Fig. 1B).

The proximity of *zy43* and *zy44* to the *arl-6* gene led us to examine DD neuron positioning in an *arl-6* mutant, but we did not observe any defects (data not shown). These mutations were also located approximately 6.5 kb upstream of *pal-1* (Fig. 1C), an essential gene encoding an orthologue of the homeobox protein CDX/Caudal, within a region known to be required for complete rescue of *pal-1* embryonic defects (Edgar et al., 2001). The CDX family of proteins are also associated with neural tube defects in mammals, suggesting *pal-1* was a good candidate for involvement in VNC formation (Savory et al., 2011).

Because strong *pal-1* loss-of-function mutants are non-viable and display severe embryonic and larval morphology defects, we asked whether the 44 bp *zy117* deletion disrupted a promoter region important for *pal-1* expression. To address this, we endogenously tagged the *pal-1* gene with a C-terminal GFP in both the WT and *zy117* background (Fig. 1E). As previously reported, PAL-1::GFP is widely expressed in the nuclei of posterior cells from the bean to 1.5-fold stage embryo (Edgar et al., 2001). Using a *cnd-1p::mCherry::PH* reporter to label the membranes of DD and DA neuronal progenitors, we observed that *PAL-1::GFP* was

also expressed in the nuclei of a subset of DD, DA, and DB progenitors, specifically those located in the posterior VNC (Fig. 1E, F). Based on their location, these appear to be DD3-6, DA3-6, and DB5-7. Strikingly, in the *zy117* promoter mutant, PAL-1::GFP expression was completely absent from DD and DA progenitors (Fig. 1G). Posterior tail cells and DB progenitors, which can be identified by their location outside and ventral to *cnd-1p*-labeled progenitors at the 1.5-fold stage, were not affected in *zy117* mutants. These results indicate that *zy43*, *zy44*, and the 44 bp *zy117* deletion mutant disrupt a *pal-1* promoter regulatory element required for expression in DD and DA neurons.

pal-1 promoter mutants exhibit motor neuron cell body positioning defects.

Our *pal-1* promoter mutants were identified based on defects in the positioning of DD motor neurons, one of three classes of motor neurons present in the VNC of newly hatched L1 worms. To quantify these position defects and determine if they extend to the other two classes of motor neurons, DA and DB, we utilised a two-colour reporter background in which each neuron class was uniquely labeled with a class-specific fluorescent cell fate marker at L1 (Saharkhiz et al., 2024). The nuclei of DD1-6 were labeled in red with *zySi2[unc-30p::mCherry::H2B]*, DA1-9 in green with *unc-4(zy123[unc-4::mNG])*, and DB1-7 in both red and green (appearing yellow) with *vab-7(zy142[vab-7::mNG::T2A::mScarlet-I::H2B])*. The *unc-4* marker also labels the interneurons SABVL, SABVR, and SABD, which are located anterior to DA1. Neuron positions were normalized by setting SABVL as the anterior reference point (0%) and the rectum as the posterior reference point (100%), allowing neuron locations to be compared relative to VNC length across different animals. When plotted, neurons of each class are numbered sequentially from anterior to posterior, regardless of their terminal cell lineage identity, which may be unknown in mutant backgrounds.

DD, DA, and DB motor neurons are stereotypically positioned and arranged in a repeating pattern along the VNC. We found that the mean position of most DD neurons in *pal-1(zy117)* showed significant anterior shifts along the VNC compared to WT (Fig. 2A and B, Fig. S1). Some DA and DB neurons were also mispositioned compared to WT, but these shifts were milder than the DD neuron defects and may represent secondary effects caused by the mispositioned DD neurons. Indeed, the strongest position shifts affected DD3–6, which correlates with *pal-1* expression in these neurons, while milder shifts were observed in DD1 and DD2, where expression is absent. In addition, except for DA8 and DA9, which are located across from each other on the left and right in the preanal ganglia, the neuron classes are arranged in an alternating sequence, with no two classes adjacent to each other (Fig. 2C-E). This pattern is significantly altered in *zy117* mutants (Fig. 2D and E). Motor neurons of the same class are also more frequently adjacent to each other. For example, in 21% of *zy117* larvae (N=53), the DD2 and DD3 cell bodies are adjacent with no intervening cells, compared to 0% in WT (N=51). Notably, although *pal-1* regulates cell fates (Edgar et al., 2001; Maduro et al., 2005), we did not observe any changes in DD, DA, or DB cell numbers that would suggest alterations in cell fate. Overall, these results indicate that *pal-1* expression, driven by the DD-DA-specific promoter element, is primarily required for proper DD motor neuron positioning.

PAL-1 acts with VANG-1 and SAX-3 to position motor neurons in the VNC.

We previously showed that the PCP pathway component VANG-1 and the Robo receptor SAX-3 act in parallel to regulate motor neuron cell body positioning in the VNC of newly hatched larvae. Loss of both *vang-1* and *sax-3* causes a highly penetrant anterior displacement of motor

neuron cell bodies, a defect that is synergistically more severe than in either single mutant (Shah et al., 2017). This pronounced anterior shift reflects a major disruption of embryonic convergent extension movements in neuronal progenitors, which converge mediolaterally and extend posteriorly along the anterior-posterior axis during VNC formation (Shah et al., 2017).

To investigate genetic interactions between *pal-1* and these pathways, we examined the VNC positions of DD and DA neurons relative to SABVL and the rectum in *pal-1(zy117)* double mutants with *vang-1(tm1422)* and *sax-3(zy5)* (Fig. 3A). *tm1422* is a deletion allele predicted to eliminate VANG-1 activity, whereas *zy5* is a nonsense allele expected to produce a SAX-3 protein with a truncated cytoplasmic domain (Shah et al., 2017). The *zy5* allele is used instead of the *sax-3* null allele because it exhibits significantly higher viability and fewer body morphology defects, which would otherwise interfere with measurements of neuron position. We found that the anterior shifts in the mean position of DD3-6 cell bodies along the VNC in *pal-1(zy117)* mutants were substantially more severe than those in *vang-1* and *sax-3* single mutants (Fig. 3B and Fig. S2). In contrast, the anterior shifts in DA cell bodies were similar across all mutants, being relatively mild in each case. *vang-1; pal-1* double mutants exhibited significantly more severe anterior shifts in mean DD and DA neuron positions compared to either single mutant. Interestingly, in *sax-3; pal-1* double mutants, the mean position of DD cell bodies showed significantly more severe anterior shifts compared to single mutants, while only DA3 and DA4 among the DA cell bodies were significantly different from *pal-1* mutants (Fig. 3B and Fig. S3). These results suggest that, at least for some aspects, *pal-1* and *vang-1* act in independent pathways to position DD and DA cell bodies. This redundancy is particularly evident in DA neurons which show a synergistic increase in the anterior shifts of mean cell body position compared to the single mutants. The findings also suggest that *pal-1* and *sax-3* act in independent pathways to position DD neurons and a subset of DA neurons. Furthermore, the similarity of the *vang-1; pal-1* cell body position phenotype to the *vang-1; sax-3* phenotype, in which convergent extension is disrupted, suggests that the downstream transcriptional targets of *pal-1* also play a partially redundant role in convergent extension.

sex-1 mutants exhibit motor neuron cell body positioning defects.

sex-1 encodes a 534-amino acid nuclear hormone receptor that was originally identified for its key role in sex determination (Carmi et al., 1998). In the same screen that identified *pal-1(zy43)* and *pal-1(zy44)*, we also isolated a *sex-1* mutant with abnormally close spacing between DD2 and DD3 cell bodies, like the defects observed in *pal-1* mutants (Fig. 4A). This mutation, *sex-1(zy45)*, introduces a premature stop codon at amino acid W51, predicted to result in a severely truncated protein. We confirmed that *sex-1* was the causative gene by observing the same motor neuron positioning defects in two additional CRISPR/Cas9-generated *sex-1* alleles: *zy130*, a 7-nucleotide deletion causing a frameshift after L54, and *zy159*, a 20-nucleotide deletion causing a frameshift after V253. These alleles were originally generated to study unrelated axon guidance defects (unpublished). Given that *pal-1* and *sex-1* show a similar DD2–DD3 cell body proximity phenotype, we investigated the role of *sex-1* in neuronal positioning.

To better understand motor neuron positioning defects in *sex-1(zy130)* mutants, we used our neuron class-specific reporters to measure the positions of DD and DA cell bodies in the newly hatched VNC relative to SABVL and the rectum. *sex-1* mutants show significant anterior shifts in the positions of both DD and DA cell bodies compared to WT, in contrast to *pal-1(zy117)* mutants, which primarily affect DD neurons (Fig. 4B and C). These DD and DA cell

body shifts become significantly more severe in *sex-1; pal-1* double mutants compared to either single mutant (Fig 4C and Fig S4). As in *pal-1* mutants, cell body position shifts in *sex-1* mutants are associated with changes to the stereotypical arrangement of motor neurons along the VNC (Fig. 4D). However, unlike *pal-1* mutants, *sex-1* mutants also display additional organizational defects in the anterior VNC, where cell bodies are frequently mispositioned dorsally rather than aligned in a single file (Fig. 4E-G). The proportion of dorsally mispositioned neurons increased from 5.9% in WT to 64.3% in *sex-1(zy130)* mutants ($p < 0.001$) (Fig. 4G). These mispositioning defects are not further enhanced in the double mutants. Together, these findings indicate that, at least for some aspects, *pal-1* and *sex-1* act redundantly or independently to position motor neurons in the VNC. Furthermore, *sex-1* plays an additional role in ensuring the single-file alignment of neurons in the anterior region of the VNC.

SEX-1 regulates PAL-1 expression in DD and DA neuronal progenitors.

Motor neuron positioning defects in the VNC of newly hatched worms indicate a disruption in the assembly of the VNC that begins at the embryonic bean stage. VNC assembly involves several distinct processes, including convergent extension of DD, DA, and DB neuronal progenitors, as well as still-unknown sorting and spacing mechanisms that establish their stereotypical organization (Shah et al., 2017; Saharkhiz et al., 2024). The increased severity of neuron positioning defects in *sex-1; pal-1* double mutants compared to single mutants suggests that *sex-1* and *pal-1* may act in parallel or independent pathways during VNC assembly, though a role in the same pathway for some aspect of this process cannot be excluded. Given that both *sex-1* and *pal-1* encode transcription factors, we tested the possibility that one might regulate the expression of the other.

We first tested whether *pal-1* regulates *sex-1* expression. To do this, we knocked mNeonGreen (mNG) into the C-terminus of *sex-1* and examined its expression in WT and *pal-1(zy117)* mutant backgrounds, using an mCherry membrane reporter to label DD and DA neurons. SEX-1::mNG was broadly expressed through the comma stage, including in the nuclei of all DD, DA, and DB progenitors (Fig. S5). Its expression declined by the 1.5-fold stage, with few nuclei still showing detectable signal. No differences in SEX-1::mNG expression were observed in the *pal-1(zy117)* mutant background.

We next tested whether *sex-1* regulates *pal-1* expression. PAL-1::GFP is normally expressed and localized to the nuclei of a subset of DD, DA, and DB progenitors. In the *sex-1(zy130)* null background, PAL-1::GFP was absent from DD and DA progenitors but remained unaffected in DB progenitors at both the bean and 1.5-fold stages (Fig. 5A). To confirm these observations, we next quantified PAL-1::GFP expression based on whether it was co-expressed with *cnd-1* (DD and DA) or not co-expressed (DB and tail cells). To do this, we used Imaris tools to segment PAL-1::GFP nuclear expression. These nuclei were then grouped based on whether they expressed *cnd-1* or not, and the mean sum intensity per cell was compared across genotypes. We found that the average intensity of PAL-1::GFP in *cnd-1*$^{+}$ nuclei was dramatically reduced in embryos carrying the 44 bp *pal-1* promoter deletion and in both *sex-1* mutants (Fig. 5B). In contrast, *cnd-1*$^{-}$ nuclei showed no significant change. This difference in intensity reflects the number of PAL-1::GFP positive nuclei detected in each region (Fig. 5C). We further showed that this regulation occurs at the level of *pal-1* transcription by showing reduced GFP expression in embryos carrying a transgene driven by the *pal-1* promoter (Fig. 5D). These findings indicate

that PAL-1 expression in DD and DA neuronal progenitors requires transcriptional regulation by SEX-1.

If PAL-1 functions downstream of SEX-1, then expressing *pal-1* from a heterologous promoter active in VNC progenitors should bypass the requirement for *sex-1* and rescue the defects observed in *sex-1* mutants. To test this, we constructed a transgene in which the *pal-1* coding sequence is driven by the *bar-1* promoter, which is also active in DD and DA progenitors (Chan et al., 2025). This construct successfully rescued *zy117* defects and caused only minimal position defects when overexpressed in WT animals (Fig. 5E and F). When introduced into a *sex-1(zy130)* mutant background, the transgene was able to partially rescue neuronal positioning defects (Fig. 5E and G). These results are consistent with *pal-1* acting downstream of *sex-1* and, in agreement with our double mutant analysis, suggest that it is likely one of multiple targets through which SEX-1 mediates its effects on neuronal positioning.

Discussion

The integration of multiple signaling pathways is key to proper nervous system development. *Caudal* homeobox (HOX) transcription factors, including the CDX family member in mammals and PAL-1 in *C. elegans,* act as key integrators of signaling pathways and are widely required for morphogenesis and cell-fate decisions during embryogenesis (van den Akker et al., 2002; Wilson et al., 2003; Palmer et al., 2021; Zhao et al., 2022). This includes early neural development, which depends on transcription that is activated by retinoic acid, WNT, and HOX transcription factors (Nordström et al., 2006; Skromne et al., 2007; Young et al., 2009; Sturgeon et al., 2011; Sanchez-Ferras et al., 2016). Several of these transcriptional mechanisms play important roles in neurulation through CDX members (Keenan et al., 2006; Savory et al., 2011; Kam et al., 2013). Loss of both *Cdx1* and *Cdx2*, results in the severe neural tube defect craniorachischisis (Savory et al., 2011; Zhao et al., 2014). In this study, we identify the nematode *Caudal* homolog PAL-1 as a key regulator of VNC development and show that NHR-mediated control of *pal-1* expression is critical for its function.

Loss of all PAL-1 activity results in embryonic lethality due to defects in cell differentiation programs and morphology (Edgar et al., 2001). We identified a regulatory element upstream of the *pal-1* promoter that controls expression in DD and DA progenitors. Disruption of this region does not cause lethality; instead, we found it leads to motor neuron position defects in the VNC of newly hatched larvae. While defects were observed in all three motor neuron classes (DD, DA and DB), loss of this promoter element primarily affected DD neurons. We determined that these defects were not due to incorrect cell fates, suggesting a failure of cell movements during embryonic development of the VNC. This observation is consistent with the role of *pal-1* promoter regions in other developmental processes. For example, tissue-specific loss of *pal-1* in a subset of ventral hypodermal cells, leads to defects in cell migration and intercalation during late embryogenesis (Gilbert et al., 2020). The role of *pal-1* in cell movements during development also parallels its involvement in other developmental processes. PAL-1 is required for the migration of several populations of dorsal hypodermal cells (Edgar et al., 2001). The broad role of PAL-1 across multiple specific cell movements, may indicate that these tissues share common mechanism. Studies on PAL-1 function have identified

several targets that promote its activity in intestinal cells and body wall muscles (lineages derived from the C blastomere), which may also play a role in neuronal cells (Baugh et al., 2005; Gilbert et al., 2020). These targets include the nuclear hormone receptors *nhr-25* and *nhr-60* and homeobox (HOX) transcription factors *ceh-16* and *mab-21,* which all have been shown to regulate morphogenetic processes during embryogenesis (Chow et al., 1995; Chen et al., 2004; Cassata et al., 2005; Baugh et al., 2005; Šimečková et al., 2007). Similarly, the T-box transcription factors *tbx-8*, *tbx-9,* and the HOX transcription factor *vab-7* are involved in patterning posterior cells through regulation of adherens junctions (Pocock et al., 2004; Sawyer et al., 2011). Whether any of these factors are direct targets of PAL-1 within the developing VNC remains to be investigated.

Components of the PCP pathway have conserved roles in both mammalian neuration and embryonic VNC development (Doudney et al., 2005; Ciruna et al., 2006; Ybot-Gonzalez et al., 2007; Shah et al., 2017; reviewed in Shi, 2022). Disruption of PCP components, including Vang1, Prickle, Scribble1 and PTK7 produce severe neural tube defects (Yen et al., 2009; Bosoi et al., 2011; Robinson et al., 2012; Tian et al., 2020). In mammals, PCP signalling during neurulation is, in part, regulated by CDX family members (Savory et al., 2011; Zhao et al., 2014). We have previously also shown that the PCP components *vang-1* and *prkl-1* are required for rosette mediated-convergent extension during VNC assembly (Shah et al., 2017). *vang-1; pal-1* double mutants exhibit more severe neuronal position defects than either single mutant. This suggests that PAL-1 does not act solely through the PCP pathway in *C. elegans*. These differences may reflect the complexity of PCP signaling and how individual components are conserved across species. The regulation of the PCP pathway by CDX proteins during mammalian neurulation involves the components PTK7 which does not have a homolog in nematodes (Savory et al., 2011). A similar increase in VNC motor neuron displacement was observed in *sax-3; pal-1* double mutants. Previous work has shown that SAX-3 functions in parallel to the PCP pathway (Shah et al., 2017). Thus, the finding that displacement of neurons is enhanced in both *pal-1* double mutants, suggests that PAL-1 may function through an additional pathway.

The expression of transcriptional enhancers and suppressors is regulated in tightly controlled spatial and temporal patterns (Ong and Corces, 2011; Panigrahi and O'Malley, 2021). This includes *cdx* genes, which have roles in diverse cell types and processes. Expression of *cdx* genes commence in the primitive streak and tail bud early during post-implantation before expanding to neuroectoderm and mesodermal tissues, finally decreasing by late gestation (Meyer and Gruss, 1993; Beck et al., 1995; Chawengsaksophak et al., 1997; Benahmed et al., 2008). The initiation, maintenance and pattern of expression across multiple *cdx* members requires diverse mechanisms, including autoregulation, traditional signaling cascades and a collective of transcription factors (Houle et al., 2003; Beland et al., 2004; Wang and Shashikant, 2007; Benahmed et al., 2008; Chang et al., 2016; Zhao et al., 2014). *pal-1* is similarly regulated in a complex manner, with temporal and spatial expression across multiple cell lineages (Hunter and Kenyon, 1996; Mootz et al., 2004; Edgar et al., 2001; Mainpal et al., 2011; Gilbert et al., 2020). This tightly regulated pattern is facilitated through multiple regulatory regions, including a fragment of exon 5 which specifically promotes *pal-1* transcription in ventral hypodermal cells (Gilbert et al., 2020). Our work builds on this by identifying a region approximately10kb upstream of the start site that is required for expression in DD and DA neurons. Tight spatial regulation of *pal-1* in the developing VNC is likely essential for its role in neuronal patterning.

Several pathways contribute to the regulation of CDX family members. These include the canonical WNT signaling pathway, autoregulation and the Nuclear Hormone Receptors (NHRs), ligand mediated regulatory factors (Houle et al., 2003; Beland et al., 2004; Sanchez-Ferras et al., 2012; reviewed in Bodofsky et al., 2017). Their importance includes conserved roles in cellular movements, including failure of mouse neural tube closure, border cell migration during oogenesis in *Drosophila* and ventral closure in *C. elegans* (Wendling et al., 1999; Simeckova et al., 2007; Bhattacharya and Starz-Gaiano, 2024). One prominent NHR family, the retinoic acid receptors (RARs), binds retinoic acid and mediates its signaling, playing a key role in the regulation of neurulation (Kam et al., 2013; Gur et al., 2022). This process is partly achieved through the regulation of convergent extension, which is disrupted by genetic manipulation of retinoic acid signaling. Retinoic acid has also been shown to regulate CDX1 expression through RAR proteins, which promote the expression of CDX1 during late gastrulation (Houle et al., 2003). This interaction may facilitate the activity of retinoic acid during neural tube development and has been shown to affect convergent extension (Mic et al., 2002, Wilson et al., 2003; Kam et al., 2013; Gur et al., 2022).

This study demonstrates that the nematode nuclear hormone receptor SEX-1 is required for *pal-1* expression in DD and DA progenitors. SEX-1 has previously been classified as an orphan nuclear hormone, for which no ligand has been found (Carmi et al., 1998). It primarily functions during sex determination and dosage compensation through the inhibition of the central transcription factor *xol-1*(Skipper et al., 1999; Gladden and Meyer, 2007; Meyer et al., 2010; Farboud et al., 2013). SEX-1 has some homology with the NHR1 superfamily, which includes retinoic acid receptors (RARs) (Carmi et al., 1998). The similar role that NHRs play in promoting CDX/PAL-1 aligns with their conserved role during collective cell movements. SEX-1 also shares homology with several other NHR1 families, including the orphan NHR REV-ERB, orphan retinoic acid receptor-related orphan receptor (ROR) subfamily and the NHR E78A, in *Drosophila* (Carmi et al., 1998). Although these additional families have well established roles in development, few direct links to the collective cell movements during neurulation have been identified. REV-ERBβ, for example, displays prominent expression in the floor of the neural tube and developing nervous system but functions largely in the circadian clock molecular circuit (Bonnelye et al., 1994; Ikeda et al., 2019). RORα is prominently found in developing ganglion cells in the cerebellum (Gold et al., 2003).

This study has explored the role and regulation of the *Caudal* family homolog *pal-1* during VNC assembly in *C. elegans*. The results highlight an important relationship between the nuclear hormone receptor SEX-1 and the tissue-specific regulation of *pal-1* within the ventral nerve cord. They also suggest that features of *Caudal* function may be conserved in nematodes. Given the prominent role that CDX family members during embryonic development in the neural tube and other mesodermal tissues, it is important to understand the mechanisms that influence their role and what functions are conserved across species.

Materials and Methods

Table 1: Key Resources

Reagent or resource	Source	Identifier
Chemicals, Peptides, and Recombinant Proteins		
Levamisol hydrochloride	Millipore Sigma	31742; CAS:16595-80-5
Bacterial and Virus Strains		
E. coli: OP50	Caenorhabditis Genetics Center (CGC)	RRID: WB-STRAIN:WBStrain00041969
Experimental Models: Organisms/Strains		
C. elegans: N2 (wild isolate)	CGC	
C. elegans: OU792 (unc-4(zy123[unc-4::mNG]) zySi2[unc-30p::mcherry::H2B::unc-30]; vab-7(zy142[vab7::mNG::T2A::mScarlet-I::H2B])	Saharkhiz et al., 2024	N/A
C. elegans: OU734 (unc-4(zy123[unc-4::mNG]) zySi2[unc-30p::mcherry::H2B::unc-30])	Saharkhiz et al., 2024	N/A
C. elegans: *pal-1(zy43)* III	This study	N/A
C. elegans: *pal-1(zy44)* III	This study	N/A
C. elegans: *pal-1(zy117)* III	This study	N/A
C. elegans: *sex-1(zy130) X*	A. Colavita, unpublished	N/A
C. elegans: *sex-1(zy159) X*	A. Colavita, unpublished	N/A
C. elegans: *pal-1(zy112[pal-1::GFP])* III	This study	N/A
C. elegans: *sex-1(zy133[zy133[sex-1::mNG::AID])* X	This study	N/A
C. elegans: *ynIs37[flp-13p::gfp]* III	CGC	WB Strain: NY2037; WormBase: WBStrain00029158
C. elegans: *sax-3(zy5) X*	Shah et al., 2017	N/A
C. elegans: *vang-1(ok1142) X*	CGC	WB Strain: RB1125; WormBase: WBStrain00031829
C. elegans: *zyIs36(cnd-1::PH::mCherry; myo-2p::mCherry) X*	Antonio Colavita, Shah et al., 2017	N/A

C. elegans: *zyIs40(unc-30p::gfp; cnd-1::PH::mCherry)* Unassigned linkage	This study	N/A
Oligonucleotides		
DNA Oligonucleotides	Eurofins	See Table S1 for sequences and use.
Software and Algorithms		
Zeiss Zen 3.2	Zeiss	https://www.zeiss.com/microscopy/en/products/software/zeiss-zen.html
R 4.4.2	R Core Team, 2019	N/A
ggplot2	Wilkinson, 2011	https://github.com/tidyverse/ggplot2
Imaris 10	Oxford Instruments	https://imaris.oxinst.com/

Strains and Maintenance

All strains were maintained and examined at 20ºC. The Bristol N2 strain was used as wild type (WT), along with the following alleles and transgenes: LGII: *unc-4(syb1658[unc-4::GFP])*. LGIII: *pal-1(zy43), pal-1(zy44), pal-1(zy117)*. LGX: *sex-1(zy45), sex-1(zy130), sex-1(zy159), sax-3(zy5), vang-1(tm1422), zyIs36[cnd-1p::PH::mCherry myo-2p::mCherry]*. Unassigned linkage: OU792, OU734, *zyIs40[unc-30p::gfp; cnd-1p::PH::mCherry myo-2p::mCherry]*.

***pal-1* and *sex-1* alleles**

pal-1(zy43), pal-1(zy44) and *sex-1(zy45)* were identified in a genetic screen for DD neuron position defects (A. Colavita, unpublished). Whole-genome sequencing, as described in Noblett et al. (2019), was used to identify the genes and their associated DNA lesions. Mutants were subsequently outcrossed at least three times and reverified by Sanger sequencing (performed at OHRI StemCore) using primers N35-N37 for *pal-1* (all primers listed in Supplemental Table 1).

The *pal-1(zy117)* deletion was generated via DNA repair of CRISPR-Cas9-induced double strand breaks (Waaijers et al., 2013). Briefly, the target site (GAATGTCATAATGACCTTTT) was identified using the IDT guide RNA design tool at idtdna.com. The sequence was inserted into the Cas9-sgRNA plasmid pDD162 (Addgene #47549) using the NEB Q5 Site-Directed Mutagenesis Kit to generate plasmid pAC564. Young adult worms containing the DD reporter transgene *ynIs37* were injected with a mix of 50 ng/µl of pAC564, 2.5 ng/µl of myo-2p::mCherry (pCFJ90, Addgene #19327) and pBluescript plasmid (Stratagene) to a concentration of 100 ng/µl. Progeny were screened for DD position defects that resembled those in *zy43* and *zy44*. Sequencing (OHRI StemCore) with primers N35 and N36 was used to identify the deletion. Subsequent genotyping was performed using primers N35-N37.

CRISPR-Cas9-mediated knock-ins

A GFP::3xFLAG and an mNG::AID::3xFLAG were inserted at the C-terminus of the endogenous *pal-1* and *sex-1* loci, respectively, using the CRISPR-Cas9 self-excising drug selection cassette approach described in Dickinson et al. (2015). Target sequences for *pal-1* (GTCGTGACAAACAGAAGATT) and *sex-1* (CAAAGGTGGCTAGCAGTGAA) insertions were cloned into the Cas9–sgRNA plasmid pDD162 to generate plasmids pAC487 and pAC703, respectively. The homology directed repair plasmids for *pal-1* (pAC486) and *sex-1* (pAC722) were constructed using the GFP (pDD282, Addgene #66823) and mNG::AID (pJW1582, Addgene #154312) selection cassette plasmids, respectively. The resulting knock-in alleles are *pal-1(zy112[pal-1::GFP])* and *sex-1(zy133[sex-1::mNG::AID])*.

Reporter and rescue constructs

A *pal-1p::mNG* transcriptional reporter (pAC499) was constructed using Gibson Assembly (New England Biolabs). This reporter combines approximately 1.8 kb of distal and 2.4 kb of proximal promoter elements upstream of an mNG cassette, with the pPD95.77 vector (a gift from Andrew Fire, Stanford) serving as the backbone. Primers N48-N53 were used for the assembly (Table S1).

A promoterless *pal-1::GFP* minigene plasmid (pAC936) was constructed using Gibson Assembly. This construct contains the *pal-1* genomic coding region, with introns 3 and 5 removed, fused to the *GFP::3X Flag* cassette from the endogenous knock-in allele *pal-1*(zy112). Primers N54-N61 were used for the assembly (Table S1). The *bar-1p::pal-1::GFP* rescue construct (pAC937) was made by inserting a 4.9 kb *bar-1* promoter into pAC936 using Gibson Assembly with primers N62-N65 (Table S1).

pAC499 and pAC936 were each injected at a concentration of 5 ng/µl, along with 2.5 ng/µl of *myo-2p::mCherry* (pCFJ90) and 92.5 ng/µl of pBluescript plasmid.

Embryonic Imaging

Widefield imaging was used to measure VNC rosette lifetimes. For widefield imaging, embryos were prepared as in Bao and Murray (2011). Briefly, several embryos were transferred from plates using a capillary attached to a glass pipette and mounted in a 3 µL drop of M9 containing approximately fifty 25 µm diameter polystyrene beads (Polyscience Inc.). The preparation was then sealed under a No. 1.5 coverslip using Vaseline. All widefield imaging was conducted on a Zeiss Imager M2, equipped with a Zeiss SVB-1 microscope signal distribution box/*TTL* trigger cable-controlled camera shutter to reduce phototoxicity. Single time-point images were taken across 15-30 0.5 µm slices at 63x (1.4NA). Unless otherwise stated, all images were deconvolved prior to analysis using constrained iterative deconvolution on Zen 3.2 (Zeiss) with a Gaussian algorithm, corrections for background and saturated pixels.

Quantification of motor neuron position defects in newly hatched larvae

Quantification of neuron position defects in L1 larvae was performed as follows. First stage larvae (L1) were mounted on 2% agarose pads using 200 µM levamisole (#31742, Sigma). Images were acquired using a Zeiss Imager M2, Colibri7 LED source, AxiocamHR camera and taken at 40x (1.4NA) over 5-7 0.5um slices. Brightfeild, RFP and GFP channels were acquired. Images were measured on FIJI/Image J software, version 2.14. Using the segmented line tool, the

position of each DD, DA and DB neuron (or only DD and DA neurons in OU734) was measured along the worm. These positions were then converted into percentage locations using SABVR = 0% and the anus = 100%. Each percentage location was plotted using base R, version 4.4.2 (R Core Team, 2019) and geom_jitter from the ggplot2 suite (Wilkinson, 2011).

Quantification of PAL-1 expression

Embryonic imaging of *sex-1(zy133[sex-1::mNG::AID])* and *pal-1(zy112[pal-1::GFP])* was conducted on a DM16000B Quorum Spinning Disk (Leica) with a EMCCD (Hamamatsu) camera. Single time-point images were taken at 63x (1.4NA) with a pinhole size of 50um. Images were acquired with a Brightfield exposure of 223ms, at FITC exposure of 500ms and a Cy3 exposure of 700ms, across 12 0.5um slices.

Intensity measurements of *pal-1(zy112[pal-1::GFP])* were conducted using Imaris 10 (Bitplane) after data was processed using Fiji/ImageJ. Briefly, Z-stacks were opened in their native format in Fiji/ImageJ. Both red and green channels were merged to form a composite color image, which was converted into RGB before exporting as a TIFF. Data was then imported into Imaris. Semi-automated spot detection was used to identify GFP nuclei with a XY diameter of at least 1.15 µm and a quality above 42. Spots were classified using the Imaris machine learning tool based upon the RFP channel and their proximity to the RFP labelled VNC cells. After spot creation was complete, the original GFP image was used to remove false positive spots which were outside the embryo boundary. Spots details including class and SUM Intensity were exported for statistical analysis and graphing.

Statistics

Tests and the number of samples for each dataset are indicated in individual figure legends. Parametric data was analyzed using Weltch's T-Test or an analysis of variance (ANOVA), as appropriate. Non-parametric data was analyzed using a Mann-Witchney U-Test or Kruskal-Wallis Test, as appropriate. Proportional data was compared using a Chi-squared test with Monte Carlo simulation for 10,000 replicates. When this returned a significant result, a pairwise analysis was conducted using Fisher's Exact Test with Monte Carlo simulation for 10,000 replicates, adjusted with Holm corrections for multiple comparisons. Statistics were conducted using base R, version 4.4.2 (R Core Team, 2019), the "multicomp" package for Dunnett's Multiple Comparison Test (Bretz et al., 2011) and "FSA" package for Dunn's Multiple Comparison Test (Ogle et al., 2022). Measurements related to embryonic phenotypes (expression pattern and order measurements) were scored blind to genotype using the Blind Analysis Tools plugin for Fiji/ImageJ (https://imagej.net/plugins/blind-analysis-tools).

Acknowledgements

We thank Chris Li for sharing *ynIs37*. Some strains were provided by the *Caenorhabditis* Genetics Center, which is funded National Institutes of Health Office of Research Infrastructure Programs (P40 OD010440). Data for *C. elegans* allele sequences was accessed through WormBase (http://www.wormbase.org, release WS294). The authors acknowledge the Cell Biology and Image Acquisition Core (RRID: SCR_021845) funded by the University of Ottawa, Natural Sciences and Engineering Research Council of Canada, and the Canada Foundation for Innovation. We would also like to acknowledge the assistance of StemCore Laboratories Genomics Core Facility (OHRI), RRID:SCR_012601. Studies presented in this report were

supported by a Project Grant from the Canadian Institutes of Health Research (CIHR 123513 and 156160) to A. Colavita.

Data availability

Data will be made available upon request.

Appendix A: Supplemental data

Supplementary Table 1. Oligonucleotides used in this study.

Supplementary Figure 1. Distribution of all DD, DA, and DB positions used to plot mean positions in Figure 2. (A-C) Quantification of (A) DA, (B) DB and (C) DD neuron position relative to the SABVL neuron and rectum in L1 stage worms. Data shows individual samples for the data presented in Figure 2. Neurons are plotted along the AP axis, where SABVL and the rectum mark the 0% and 100% positions respectively. Black bars represent the means and 95% confidence intervals.

Supplementary Figure 2. Distribution of all DD and DA positions used to plot mean positions in Figure 3 and 4. (A-B) Quantification of (A) DA and (B) DD neuron position relative to the SABVL neuron and rectum in L1 stage worms. Each graph shows individual samples for the data presented in Figures 3 and 4. Neurons are plotted along the AP axis, where SABVL and the rectum mark the 0% and 100% positions respectively. Black bars represent the means and 95% confidence intervals.

Supplementary Figure 3. Comparison of *pal-1(zy117)* double mutants with *vang-1(tm1422)* and *sax-3(zy5)*. (A-B) Each graph shows the mean position of DD and DA neurons in larvae as presented in Figure 3. Neurons are plotted along the AP axis, where SABVL and rectum mark the 0% and 100% positions respectively. Means and 95% confidence intervals are indicated for each neuron and animals scored (N) indicated on the right. Hashed lines indicate the mean position of WT DD neurons. Arrows indicate the size and direction of the mean neuron position shift in the double mutant from the mean neuron position in (A) *pal-1(zy117)*, (B) *vang-1(tm1422)* or *sax-3(zy5)* single mutants. Statistics: one-way ANOVA with Tukey's Post-hoc Comparisons. *p<0.05, **p<0.01, ***p<0.001.

Supplementary Figure 4. Comparison of *sex-1(zy130); pal-1(zy117)* double mutants to single mutants. (A-B) Each graph shows the mean position of DD and DA neurons in larvae as presented in Figure 4. Neurons are plotted along the AP axis, where SABVL and the rectum mark the 0% and 100% positions respectively. Means and 95% confidence intervals are indicated for each neuron and animals scored (N) indicated on the right. Hashed lines indicate the mean position of WT DD neurons. Arrows indicate the size and direction of the mean neuron position shift in the double mutant from the mean neuron position in (A) *pal-1(zy117)* or (B) *sex-1(zy130)* single mutants. Statistics: one-way ANOVA with Tukey's Post-hoc Comparisons. *p<0.05, **p<0.01, ***p<0.001.

Supplementary Figure 5. Loss of PAL-1 does not affect the expression of endogenous SEX-1::GFP. (A) Representative maximum projections of an endogenous *SEX-1::mNG* in WT and

pal-1(zy117) embryos. At the bean stage, N = 15 for both WT and *pal-1(zy117)*. At the 1.5-fold stage, N = 14 for WT and N = 15 for *pal-1(zy117)*. No visual changes are observed. Posterior *cnd-1p::RFP::PH* expression marks DD and DA neurons. The white hashed outline marks the embryo. Scale bar = 10μm.

References

van den Akker, E., Forlani, S., Chawengsaksophak, K., de Graaff, W., Beck, F., Meyer, B. I., & Deschamps, J. (2002). Cdx1 and Cdx2 have overlapping functions in anteroposterior patterning and posterior axis elongation.

Arnold, P. R., Wells, A. D., & Li, X. C. (2020). Diversity and emerging roles of enhancer RNA in regulation of gene expression and cell fate. *Frontiers in cell and developmental biology*, *7*, 377.

Asahina, M., Ishihara, T., Jindra, M., Kohara, Y., Katsura, I., & Hirose, S. (2000). The conserved nuclear receptor Ftz-F1 is required for embryogenesis, moulting and reproduction in Caenorhabditis elegans. *Genes to Cells*, *5*(9), 711-723.

Baugh, L. R., Hill, A. A., Claggett, J. M., Hill-Harfe, K., Wen, J. C., Slonim, D. K., ... & Hunter, C. P. (2005). The homeodomain protein PAL-1 specifies a lineage-specific regulatory network in the C. elegans embryo.

Bao, Z., & Murray, J. I. (2011). Mounting Caenorhabditis elegans embryos for live imaging of embryogenesis. *Cold Spring Harbor Protocols*, *2011*(9), pdb-prot065599.

Beck, F., Erler, T., Russell, A., & James, R. (1995). Expression of Cdx-2 in the mouse embryo and placenta: possible role in patterning of the extra-embryonic membranes. *Developmental Dynamics*, *204*(3), 219-227.

Belakavadi, M., & Fondell, J. D. (2006). Role of the mediator complex in nuclear hormone receptor signaling. *Reviews of physiology, biochemistry and pharmacology*, 23-43.

Béland, M., Pilon, N., Houle, M., Oh, K., Sylvestre, J. R., Prinos, P., & Lohnes, D. (2004). Cdx1 autoregulation is governed by a novel Cdx1-LEF1 transcription complex. *Molecular and cellular biology*, *24*(11), 5028-5038.

Benahmed, F., Gross, I., Gaunt, S. J., Beck, F., Jehan, F., Domon–Dell, C., ... & Duluc, I. (2008). Multiple regulatory regions control the complex expression pattern of the mouse Cdx2 homeobox gene. *Gastroenterology*, *135*(4), 1238-1247.

Bhattacharya, M., & Starz-Gaiano, M. (2024). Steroid hormone signaling synchronizes cell migration machinery, adhesion and polarity to direct collective movement. *Journal of Cell Science*, *137*(5), jcs261164.

Bodofsky, S., Koitz, F., & Wightman, B. (2017). Conserved and exapted functions of nuclear receptors in animal development. *Nuclear receptor research*, *4*, 101305.

Bosoi, C. M., Capra, V., Allache, R., Trinh, V. Q. H., De Marco, P., Merello, E., ... & Kibar, Z. (2011). Identification and characterization of novel rare mutations in the planar cell polarity gene PRICKLE1 in human neural tube defects. *Human mutation*, *32*(12), 1371-1375.

Bonnelye, E., Vanacker, J. M., Desbiens, X., Begue, A., Stehelin, D., & Laudet, V. (1994). Rev-erbb, a new member of the nuclear receptor superfamily, is expressed in the nervous system during chicken development. *Cell Growth and Differentiation-Publication American Association for Cancer Research*, *5*(12), 1357-1366.

Bretz F, Hothorn T, Westfall PH. Multiple comparisons using R. Boca Raton, FL: CRC Press; 2011.

Brožová, E., Šimečková, K., Kostrouch, Z., Rall, J. E., & Kostrouchová, M. (2006). NHR-40, a Caenorhabditis elegans supplementary nuclear receptor, regulates embryonic and early larval development. *Mechanisms of development*, *123*(9), 689-701.

Carmi, I., Kopczynski, J. B., & Meyer, B. J. (1998). The nuclear hormone receptor SEX-1 is an X-chromosome signal that determines nematode sex. *Nature*, *396*(6707), 168-173.

Cassata, G., Shemer, G., Morandi, P., Donhauser, R., Podbilewicz, B., & Baumeister, R. (2005). ceh-16/engrailed patterns the embryonic epidermis of Caenorhabditis elegans.

Chan, W., Evans, J., Roenspies, T., Rumley, J. D., Murray, J. I., & Colavita, A. (2025). Notch-mediated regulation of β-Catenin-TCF activity instructs anteroposterior neuron positioning in C. elegans. *bioRxiv*, https://doi.org/10.1101/2025.03.02.641079.

Chang, J., Skromne, I., & Ho, R. K. (2016). CDX4 and retinoic acid interact to position the hindbrain–spinal cord transition. *Developmental biology*, *410*(2), 178-189.

Chawengsaksophak, K. (2019). Cdx2 animal models reveal developmental origins of cancers. *Genes*, *10*(11), 928.

Chen, Z., Eastburn, D. J., & Han, M. (2004). The Caenorhabditis elegans nuclear receptor gene nhr-25 regulates epidermal cell development. *Molecular and cellular biology*, *24*(17), 7345-7358.

Chow, K. L., Hall, D. H., & Emmons, S. W. (1995). The mab-21 gene of Caenorhabditis elegans encodes a novel protein required for choice of alternate cell fates. *Development*, *121*(11), 3615-3626.

Ciruna, B., Jenny, A., Lee, D., Mlodzik, M., & Schier, A. F. (2006). Planar cell polarity signalling couples cell division and morphogenesis during neurulation. *Nature*, *439*(7073), 220-224.

Davis, M. B., Jash, E., Chawla, B., Haines, R. A., Tushman, L. E., Troll, R., & Csankovszki, G. (2022). Dual roles for nuclear RNAi Argonautes in Caenorhabditis elegans dosage compensation. *Genetics*, *221*(1), iyac033.

Devitt, C. C., Weng, S., Bejar-Padilla, V. D., Alvarado, J., & Wallingford, J. B. (2024). PCP and Septins govern the polarized organization of the actin cytoskeleton during convergent extension. *Current Biology*, *34*(3), 615-622.

Dickinson, D. J., Pani, A. M., Heppert, J. K., Higgins, C. D., & Goldstein, B. (2015). Streamlined genome engineering with a self-excising drug selection cassette. *Genetics*, *200*(4), 1035-1049.

Doudney, K., & Stanier, P. (2005, May). Epithelial cell polarity genes are required for neural tube closure. In *American Journal of Medical Genetics Part C: Seminars in Medical Genetics* (Vol. 135, No. 1, pp. 42-47). Hoboken: Wiley Subscription Services, Inc., A Wiley Company.

Dumas, K. J., Delaney, C. E., Flibotte, S., Moerman, D. G., Csankovszki, G., & Hu, P. J. (2013). Unexpected role for dosage compensation in the control of dauer arrest, insulin-like signaling, and FoxO transcription factor activity in Caenorhabditis elegans. *Genetics*, *194*(3), 619-629.

Edgar, L. G., Carr, S., Wang, H., & Wood, W. B. (2001). Zygotic expression of the caudal homolog pal-1 is required for posterior patterning in Caenorhabditis elegans embryogenesis. *Developmental biology*, *229*(1), 71-88.

Farboud, B., Nix, P., Jow, M. M., Gladden, J. M., & Meyer, B. J. (2013). Molecular antagonism between X-chromosome and autosome signals determines nematode sex. *Genes & development*, *27*(10), 1159-1178.

Frankel, N. (2012). Multiple layers of complexity in cis-regulatory regions of developmental genes. *Developmental Dynamics*, *241*(12), 1857-1866.

Gilbert, S. P., Mullan, T. W., Poole, R. J., & Woollard, A. (2020). Caudal-dependent cell positioning directs morphogenesis of the C. elegans ventral epidermis. *Developmental Biology*, *461*(1), 31-42.

Gladden, J. M., & Meyer, B. J. (2007). A ONECUT homeodomain protein communicates X chromosome dose to specify Caenorhabditis elegans sexual fate by repressing a sex switch gene. *Genetics*, *177*(3), 1621-1637.

Gold, D. A., Baek, S. H., Schork, N. J., Rose, D. W., Larsen, D. D., Sachs, B. D., ... & Hamilton, B. A. (2003). RORα coordinates reciprocal signaling in cerebellar development through sonic hedgehog and calcium-dependent pathways. *Neuron*, *40*(6), 1119-1131.

Gur, M., Edri, T., Moody, S. A., & Fainsod, A. (2022). Retinoic acid is required for normal morphogenetic movements during gastrulation. *Frontiers in cell and developmental biology*, *10*, 857230.

Hayes, M., Naito, M., Daulat, A., Angers, S., & Ciruna, B. (2013). Ptk7 promotes non-canonical Wnt/PCP-mediated morphogenesis and inhibits Wnt/β-catenin-dependent cell fate decisions during vertebrate development. *Development*, *140*(8), 1807-1818.

Houle, M., Sylvestre, J. R., & Lohnes, D. (2003). Retinoic acid regulates a subset of Cdx1 function in vivo.

Hunter, C. P., & Kenyon, C. (1996). Spatial and temporal controls target pal-1 blastomere-specification activity to a single blastomere lineage in C. elegans embryos. *Cell*, *87*(2), 217-226.

Ikeda, R., Tsuchiya, Y., Koike, N., Umemura, Y., Inokawa, H., Ono, R., ... & Yagita, K. (2019). REV-ERBα and REV-ERBβ function as key factors regulating Mammalian Circadian Output. *Scientific reports*, *9*(1), 10171.

Jash, E., Tan, Z. M., Rakozy, A. I., Azhar, A. A., Mendoza, H., & Csankovszki, G. (2024). Multi-level transcriptional regulation of embryonic sex determination and dosage compensation by the X-signal element sex-1. *bioRxiv*.

Kam, R. K. T., Shi, W., Chan, S. O., Chen, Y., Xu, G., Bik-San Lau, C., ... & Zhao, H. (2013). Dhrs3 protein attenuates retinoic acid signaling and is required for early embryonic patterning. *Journal of Biological Chemistry*, *288*(44), 31477-31487.

Keenan, I. D., Sharrard, R. M., & Isaacs, H. V. (2006). FGF signal transduction and the regulation of Cdx gene expression. *Developmental biology*, *299*(2), 478-488.

Keller, M. S., Ezaki, T., Guo, R. J., & Lynch, J. P. (2004). Cdx1 or Cdx2 expression activates E-cadherin-mediated cell-cell adhesion and compaction in human COLO 205 cells. *American Journal of Physiology-Gastrointestinal and Liver Physiology*, *287*(1), G104-G114.

Khan, S. H., & Okafor, C. D. (2022). Interactions governing transcriptional activity of nuclear receptors. *Biochemical Society Transactions*, *50*(6), 1941-1952.

Kwon, J. Y., Park, J. M., Gim, B. S., Han, S. J., Lee, J., & Kim, Y. J. (1999). Caenorhabditis elegans mediator complexes are required for developmental-specific transcriptional activation. *Proceedings of the National Academy of Sciences*, *96*(26), 14990-14995.

Lees, J. A., Fawell, S. E., White, R., & G. Parker, M. (1990). A 22-amino-acid peptide restores DNA-binding activity to dimerization-defective mutants of the estrogen receptor. *Molecular and cellular biology*, *10*(10), 5529-5531.

Li, L., & Wunderlich, Z. (2017). An enhancer's length and composition are shaped by its regulatory task. *Frontiers in genetics*, *8*, 63.

Lorentz, O., Duluc, I., Arcangelis, A. D., Simon-Assmann, P., Kedinger, M., & Freund, J. N. (1997). Key role of the Cdx2 homeobox gene in extracellular matrix–mediated intestinal cell differentiation. *Journal of Cell Biology*, *139*(6), 1553-1565.

Ludewig, A. H., Kober-Eisermann, C., Weitzel, C., Bethke, A., Neubert, K., Gerisch, B., ... & Antebi, A. (2004). A novel nuclear receptor/coregulator complex controls C. elegans lipid metabolism, larval development, and aging. *Genes & development*, *18*(17), 2120-2133.

Lu, Y., Ahamed, T., Mulcahy, B., Meng, J., Witvliet, D., Guan, S. A., Holmyard, D., Hung, W., Wen, Q., Chisholm, A. D., Samuel, A. D. T., & Zhen, M. (2022). Extrasynaptic signaling enables an asymmetric juvenile motor circuit to produce symmetric undulation. Current biology: CB, **32**(21), 4631–4644.e5. doi:10.1016/j.cub.2022.09.002.

Maduro, M. F., Kasmir, J. J., Zhu, J., & Rothman, J. H. (2005). The Wnt effector POP-1 and the PAL-1/Caudal homeoprotein collaborate with SKN-1 to activate C. elegans endoderm development. *Developmental biology*, *285*(2), 510-523.

Mainpal, R., Priti, A., & Subramaniam, K. (2011). PUF-8 suppresses the somatic transcription factor PAL-1 expression in C. elegans germline stem cells. *Developmental biology*, *360*(1), 195-207.

Martinez, S., Scerbo, P., Giordano, M., Daulat, A. M., Lhoumeau, A. C., Thomé, V., ... & Borg, J. P. (2015). The PTK7 and ROR2 protein receptors interact in the vertebrate WNT/planar cell polarity (PCP) pathway. *Journal of Biological Chemistry*, *290*(51), 30562-30572.

Mic, F. A., Haselbeck, R. J., Cuenca, A. E., & Duester, G. (2002). Novel retinoic acid generating activities in the neural tube and heart identified by conditional rescue of Raldh2 null mutant mice.

Meyer, B. I., & Gruss, P. (1993). Mouse Cdx-1 expression during gastrulation. *Development*, *117*(1), 191-203.

Meyer, B. J. (2010). Targeting X chromosomes for repression. *Current opinion in genetics & development*, *20*(2), 179-189.

Mootz, D., Ho, D. M., & Hunter, C. P. (2004). The STAR/Maxi-KH domain protein GLD-1 mediates a developmental switch in the translational control of C. elegans PAL-1.

Mulcahy, B., Witvliet, D. K., Mitchell, J., Schalek, R., Berger, D. R., Wu, Y., Holmyard, D., Lu, Y., Ahamed, T., Samuel, A. D. T., Chisholm, A. D., Lichtman, J. W., & Zhen, M. (2022). Post-embryonic remodeling of the C. elegans motor circuit. *Current biology : CB*, *32*(21), 4645–4659.e3. https://doi.org/10.1016/j.cub.2022.09.065

Noblett, N., Wu, Z., Ding, Z. H., Park, S., Roenspies, T., Flibotte, S., ... & Colavita, A. (2019). DIP-2 suppresses ectopic neurite sprouting and axonal regeneration in mature neurons. *Journal of Cell Biology*, *218*(1), 125-133.

Noblett, N., Roenspies, T., Flibotte, S., & Colavita, A. (2024). IPPK-1 and IP6 contribute to ventral nerve cord assembly in C. elegans. *bioRxiv*, 2024-03.

Nordström, U., Maier, E., Jessell, T. M., & Edlund, T. (2006). An early role for WNT signaling in specifying neural patterns of Cdx and Hox gene expression and motor neuron subtype identity. *PLoS biology*, *4*(8), e252.

Ong, C. T., & Corces, V. G. (2011). Enhancer function: new insights into the regulation of tissue-specific gene expression. *Nature Reviews Genetics*, *12*(4), 283-293.

Ogle, D. H., Wheeler, P., & Dinno, A. (2022). *FSA: Fisheries Stock Analysis; R Package Version 0.8. 32. 2021*.

Palmer, A. J., Savery, D., Massa, V., Copp, A. J., & Greene, N. D. (2021). Genetic interaction of Pax3 mutation and canonical Wnt signaling modulates neural tube defects and neural crest abnormalities. *Genesis*, *59*(11), e23445.

Panigrahi, A., & O'Malley, B. W. (2021). Mechanisms of enhancer action: the known and the unknown. *Genome biology*, *22*(1), 108.

Pocock, R., Ahringer, J., Mitsch, M., Maxwell, S., & Woollard, A. (2004). A regulatory network of T-box genes and the even-skipped homologue vab-7 controls patterning and morphogenesis in C. elegans.

R Core Team (2019) R: a language and environment for statistical computing. R Foundation for Statistical Computing, Vienna, Austria. https://www.R-project.org.

Robinson, A., Escuin, S., Doudney, K., Vekemans, M., Stevenson, R. E., Greene, N. D., ... & Stanier, P. (2012). Mutations in the planar cell polarity genes CELSR1 and SCRIB are associated with the severe neural tube defect craniorachischisis. *Human mutation*, *33*(2), 440-447.

Saharkhiz, S., Petite, M., Roenspies, T., Perkins, T., & Colavita, A. (2024). VNC-Dist: A machine learning-based pipeline for quantification of neuronal positioning in the ventral nerve cord of C. elegans. bioRxiv, https://doi.org/10.1101/2024.11.16.623955.

Sanchez-Ferras, O., Bernas, G., Farnos, O., Touré, A. M., Souchkova, O., & Pilon, N. (2016). A direct role for murine Cdx proteins in the trunk neural crest gene regulatory network. *Development*, *143*(8), 1363-1374.

Savory, J. G., Mansfield, M., Rijli, F. M., & Lohnes, D. (2011). Cdx mediates neural tube closure through transcriptional regulation of the planar cell polarity gene Ptk7. *Development*, *138*(7), 1361-1370.

Sawyer, J. K., Choi, W., Jung, K. C., He, L., Harris, N. J., & Peifer, M. (2011). A contractile actomyosin network linked to adherens junctions by Canoe/afadin helps drive convergent extension. *Molecular biology of the cell*, *22*(14), 2491-2508.

Shah, P. K., Tanner, M. R., Kovacevic, I., Rankin, A., Marshall, T. E., Noblett, N., ... & Colavita, A. (2017). PCP and SAX-3/Robo pathways cooperate to regulate convergent extension-based nerve cord assembly in C. elegans. *Developmental cell*, *41*(2), 195-203.

Shi, D. L. (2022). Wnt/planar cell polarity signaling controls morphogenetic movements of gastrulation and neural tube closure. *Cellular and Molecular Life Sciences*, *79*(12), 586.

Shindo, A., Inoue, Y., Kinoshita, M., & Wallingford, J. B. (2019). PCP-dependent transcellular regulation of actomyosin oscillation facilitates convergent extension of vertebrate tissue. *Developmental biology*, *446*(2), 159-167.

Šimečková, K. (2007). Nuclear receptors in Caenorhabditis elegans: NHR-60 regulates embryonic development.

Skipper, M., Milne, C. A., & Hodgkin, J. (1999). Genetic and molecular analysis of fox-1, a numerator element involved in Caenorhabditis elegans primary sex determination. *Genetics*, *151*(2), 617-631.

Skromne, I., Thorsen, D., Hale, M., Prince, V. E., & Ho, R. K. (2007). Repression of the hindbrain developmental program by Cdx factors is required for the specification of the vertebrate spinal cord.

Sturgeon, K., Kaneko, T., Biemann, M., Gauthier, A., Chawengsaksophak, K., & Cordes, S. P. (2011). Cdx1 refines positional identity of the vertebrate hindbrain by directly repressing Mafb expression. *Development*, *138*(1), 65-74.

Taneja, R., Rochette-Egly, C., Plassat, J. L., Penna, L., Gaub, M. P., & Chambon, P. (1997). Phosphorylation of activation functions AF-1 and AF-2 of RARα and RARγ is indispensable for differentiation of F9 cells upon retinoic acid and cAMP treatment. *The EMBO journal*.

Tian, T., Lei, Y., Chen, Y., Guo, Y., Jin, L., Finnell, R. H., ... & Ren, A. (2020). Rare copy number variations of planar cell polarity genes are associated with human neural tube defects. *neurogenetics*, *21*, 217-225.

Waaijers, S., & Boxem, M. (2014). Engineering the Caenorhabditis elegans genome with CRISPR/Cas9. *Methods*, *68*(3), 381-388.

Wang, W. C., & Shashikant, C. S. (2007). Evidence for positive and negative regulation of the mouse Cdx2 gene. *Journal of Experimental Zoology Part B: Molecular and Developmental Evolution*, *308*(3), 308-321.

Waring, D. A., & Kenyon, C. (1991). Regulation of cellular responsiveness to inductive signals in the developing C. elegans nervous system. *Nature*, *350*(6320), 712-715.

Webster, C. M., Wu, L., Douglas, D., & Soukas, A. A. (2013). A non-canonical role for the C. elegans dosage compensation complex in growth and metabolic regulation downstream of TOR complex 2. *Development*, *140*(17), 3601-3612.

Wehner, P., Shnitsar, I., Urlaub, H., & Borchers, A. (2011). RACK1 is a novel interaction partner of PTK7 that is required for neural tube closure. *Development*, *138*(7), 1321-1327.

Wen, Q., Gao, S., & Zhen, M. (2018). Caenorhabditis elegans excitatory ventral cord motor neurons derive rhythm for body undulation. *Philosophical Transactions of the Royal Society B: Biological Sciences*, *373*(1758), 20170370.

Wendling, O., Chambon, P., & Mark, M. (1999). Retinoid X receptors are essential for early mouse development and placentogenesis. *Proceedings of the National Academy of Sciences*, *96*(2), 547-551.

Wilkinson, L. (2011). ggplot2: elegant graphics for data analysis by WICKHAM, H.

Wilson, L., Gale, E., & Maden, M. (2003). The role of retinoic acid in the morphogenesis of the neural tube. *Journal of anatomy*, *203*(4), 357-368.

Ybot-Gonzalez, P., Savery, D., Gerrelli, D., Signore, M., Mitchell, C. E., Faux, C. H., ... & Copp, A. J. (2007). Convergent extension, planar-cell-polarity signalling and initiation of mouse neural tube closure.

Yen, W. W., Williams, M., Periasamy, A., Conaway, M., Burdsal, C., Keller, R., ... & Sutherland, A. (2009). PTK7 is essential for polarized cell motility and convergent extension during mouse gastrulation.

Young, T., Rowland, J. E., van de Ven, C., Bialecka, M., Novoa, A., Carapuco, M., ... & Deschamps, J. (2009). Cdx and Hox genes differentially regulate posterior axial growth in mammalian embryos. *Developmental cell*, *17*(4), 516-526.

Zamir, I., Harding, H. P., Atkins, G. B., Hörlein, A., Glass, C. K., Rosenfeld, M. G., & Lazar, M. A. (1996). A nuclear hormone receptor corepressor mediates transcriptional silencing by receptors with distinct repression domains. *Molecular and cellular biology*, *16*(10), 5458-5465.

Zhu, Y., & Lohnes, D. (2022). Regulation of axial elongation by Cdx. *Developmental Biology*, *483*, 118-127.

Zhao, T., Gan, Q., Stokes, A., Lassiter, R. N., Wang, Y., Chan, J., ... & Zhou, C. J. (2014). β-catenin regulates Pax3 and Cdx2 for caudal neural tube closure and elongation. *Development*, *141*(1), 148-157.

Zhao, T., McMahon, M., Reynolds, K., Saha, S. K., Stokes, A., & Zhou, C. J. (2022). The role of Lrp6-mediated Wnt/β-catenin signaling in the development and intervention of spinal neural tube defects in mice. *Disease models & mechanisms*, *15*(6), dmm049517.

Figure Legends

Figure 1. A distal promoter element regulates *pal-1* expression in DD and DA progenitors. (A-B) Representative images of DD positions in (A) WT, *pal-1(zy43)*, *pal-1(zy44)* and (B) *pal-1(zy117)* mutants. Arrowheads mark DD neurons, which are visualised using *flp-13p::GFP*. Scale bar = 20μm. (C) Diagram of the *pal-1* genomic region showing the positions of mutations used in this study. (D) The location of nucleotide changes in *zy43*, *zy44* and *zy117*. Red nucleotides highlight the deleted sequence in *pal-1(zy117)*. (E) Representative maximum intensity projections of an endogenous *pal-1::GFP* expression at three stages of embryonic development. Nomarski image indicates the morphology of the embryo. A *cnd-1p::mCherry ::PH* reporter labels the membranes of DD and a subset of DA progenitors. Scale bar = 10μm. (F) Representative maximum intensity projections show endogenous *pal-1::GFP* expression in WT and *pal-1(zy117)* mutant backgrounds. The dotted line indicates regions of interest containing expression changes. Number of embryos examined: N = 8 for WT and N = 3 for *pal-1(zy117)* at the bean stage. N = 4 for both genotypes at comma stage. N = 7 for WT and N = 6 for *pal-1(zy117)* at the 1.5-fold stage. Scale bar = 10μm.

Figure 2. *pal-1* is required for proper motor neuron positioning in the VNC. (A) Representative images of DD, DA, and DB positions in WT and *pal-1(zy117)* mutants. DA neurons (*zy123[unc-4::mNG*) are indicated in green, DB neurons (*zy142[vab-7::mNG::T2A::mScarlet-I::H2B]*) in grey and DD neurons (*unc-30p::mCherry::H2B*) in magenta. Arrowheads mark the position of DD neurons. Scale bar = 20μm. (B) Quantification of DD, DA, and DB mean neuron position relative to the SABVL neuron and the rectum in L1

stage worms. Means and 95% confidence intervals are indicated for each neuron. Animals scored (N) indicated on the right. Hashed lines indicate the mean position of WT DD neurons. Arrows indicate the size and direction of the mean neuron position in *pal-1(zy117)* from the mean position of their WT equivalent. (C) Schematic of neuron organization in the L1 stage VNC. DA neurons in green and DD neurons in magenta. (D) Representative images showing neuron organization in WT and *pal-1(zy117)* mutants. Scale bar = 20μm. (E) Organization of DA, DB and DD neurons in WT and *pal-1(zy117)* worms. Individual boxes show the identity of the neuron in each position along the VNC with each row indicating an individual. The top row shows the stereotypical order of neurons in WT. Statistics: (B) Weltch's T-Test, (E) Mann Whitney U-Test. *p<0.05, **p<0.01, ***p<0.001.

Figure 3. Genetic interactions between *pal-1*, *vang-1*, and *sax-3* during neuronal positioning. (A) Representative images of WT, *pal-1(zy117)*, *vang-1(tm1422)*, *sax-3(zy5)* single and double mutants. DA neurons in green and DD neurons in magenta. Arrowheads mark the position of DD neurons. Scale bar = 20μm. (B) Quantification of DD and DA neuron position relative to the SABVL neuron and rectum in L1 stage worms. Means and 95% confidence intervals are indicated for each neuron and animals scored (N) indicated on the right. Hashed lines indicate the position of WT DD neurons. Arrows indicate the size and direction of the mean neuron position shift in each neuron compared to the mean position of their WT equivalent. Statistics: (B) one-way ANOVA with Tukey's Post-hoc Comparison. *p<0.05, **p<0.01, ***p<0.001.

Figure 4. *sex-1* is required for proper motor neuron positioning in the VNC and genetic interactions with *pal-1*. (A) Representative image of DD neuron positions in *sex-1(zy45)*, visualized using *flp-13p::GFP*. (B) Representative images of WT, *pal-1(zy117)*, *sex-1(zy130)*, and double mutants showing DA neurons in green and DD neurons in magenta. Arrowheads mark the position of DD neurons. Scale bar = 20μm. (C) Quantification of DD and DA neuron position relative to the SABVL neuron and rectum in L1 stage worms. Means and 95% confidence intervals are indicated for each neuron. Animals scored (N) indicated on the right. Hashed lines indicate the position of WT DD neurons. Arrows indicate the size and direction of the mean neuron position shift in each neuron from the mean position of their WT equivalent. (D) Organization DD and DA neurons in WT and mutant worms. (E) Schematic showing DD and DA neuron organization along the VNC. (F) Representative images of anterior DA and DD neurons in *pal-1(zy117)*, *sex-1(zy130)* and double mutants. Asterisks mark dorsally mispositioned neurons. Scale bar = 20μm. (G) Quantification of worms with dorsally mispositioned neurons at L1. Statistics: (C) one-way ANOVA with Tukey's Post-hoc Comparisons, (D) Kruskal-Wallis Test with Dunn's Post-hoc Comparisons and (G) Chi-squared test with Monte Carlo simulation for 10,000 replicates, followed by a pairwise analysis using Fisher's exact test with Monte Carlo simulation for 10,000 replicates and adjusted with Holm corrections. *p<0.05, **p<0.01, ***p<0.001.

Figure 5. SEX-1 regulates PAL-1 expression. (A) Representative maximum projection images of *PAL-1::GFP* in WT, *pal-1(zy117) and sex-1* mutant embryos at bean and 1.5-fold stage. Hashed circles indicate regions with altered expression in mutant embryos. (B-C) Quantification of the (B) mean intensity and (C) number of nuclei expressing *PAL-1::GFP* in WT, *pal-1(zy117)* and *sex-1* mutant embryos. Nuclei were grouped based on their co-expression with *cnd-1*$^{+}$ cells, labelling the VNC. Means and 95% confidence intervals are indicated for each population with individual measurements shown. At the bean stage, N = 16, 15, 11 and 15, for WT, *pal-1(zy117), sex-1(zy130)* and *sex-1(zy159*), respectively. At the 1.5-fold stage, N = 19, 13, 13 and 12, for WT, *pal-1(zy117), sex-1(zy130)* and *sex-1(zy159*), respectively. (D) Representative images showing *pal-1p::GFP* transcriptional reporter in WT or *sex-1(zy130)* background. Number of embryos examined: N = 9 for WT and N = 1 for *sex-1(zy130)*. Arrows indicate regions of interest. (E) Representative images of DD neuron positions in *pal-1(zy117)* and *sex-1(zy130)* mutants with or without a *bar-1p::PAL-1::GFP* transgene. Arrowheads mark the position of DD neurons. Scale bar = 20μm. (F and G) Quantification of DD neuron position relative to the SABVL neuron and the rectum in L1 stage (F) WT or (G) mutant worms with or without the extrachromosomal transgene. Means and 95% confidence intervals are indicated for each neuron and animals scored (N) indicated on the right. Hashed lines indicate the position of WT DD neurons. Arrows indicate the size and direction of the mean neuron position shift in each transgene expressing neuron from the mean position of their non-transgene equivalent. Statistics: (B) one-way ANOVA with Dunnet's Post-hoc Comparison, (C) Kruskal-Wallis Test with Dunn's Post-hoc Comparisons, (F-G) Weltch's T-Test. *$p<0.05$, **$p<0.01$, ***$p<0.001$.

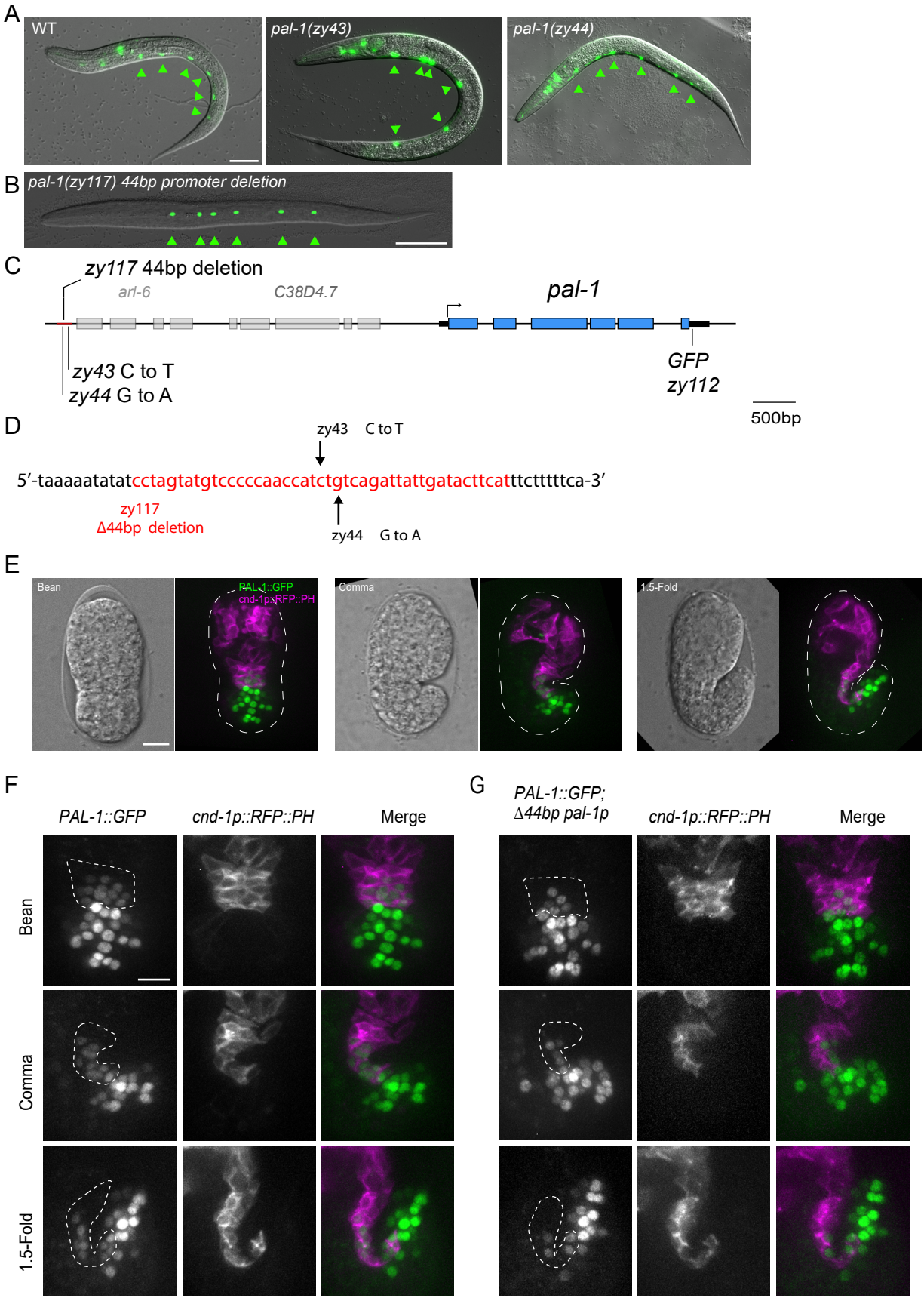
A
WT
pal-1(zy43)
pal-1(zy44)
B
pal-1(zy117) 44bp promoter deletion
C
zy117 44bp deletion
arl-6
C38D4.7
pal-1
zy43 C to T
zy44 G to A
GFP
zy112
500bp
D
zy43 C to T
5′-taaaaatatatcctagtatgtcccccaaccatctgtcagattattgatacttcatttcttttttca-3′
zy117
Δ44bp deletion
zy44 G to A
E
Bean
PAL-1::GFP
cnd-1p::RFP::PH
Comma
1.5-Fold
F
PAL-1::GFP
cnd-1p::RFP::PH
Merge
Bean
Comma
1.5-Fold
G
PAL-1::GFP;
Δ44bp pal-1p
cnd-1p::RFP::PH
Merge

FIG 1

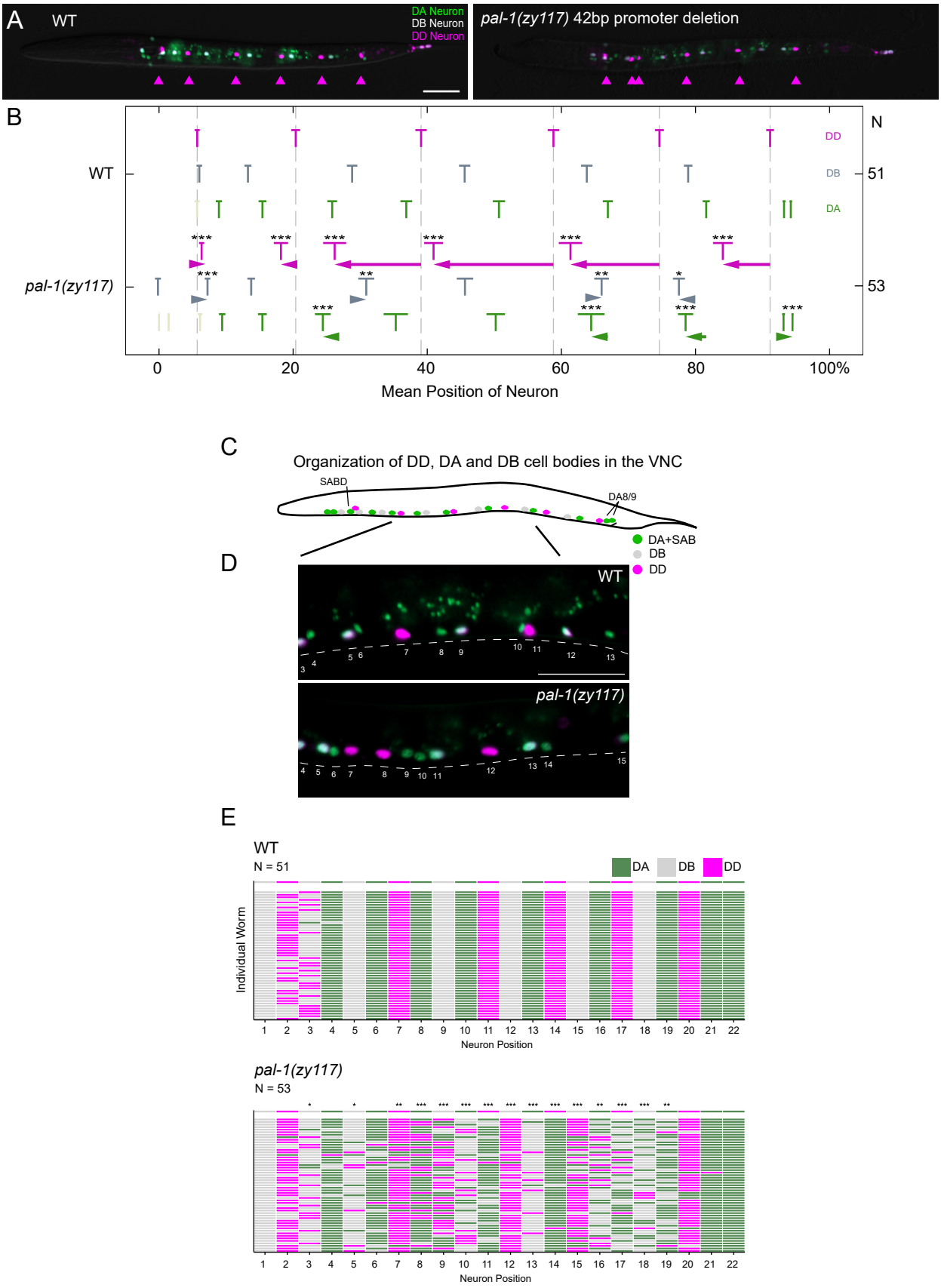
A
WT
DA Neuron
DB Neuron
DD Neuron
pal-1(zy117) 42bp promoter deletion
B
WT
pal-1(zy117)
N
DD
DB
DA
51
53
0
20
40
60
80
100%
Mean Position of Neuron
C
Organization of DD, DA and DB cell bodies in the VNC
SABD
DA8/9
DA+SAB
DB
DD
D
WT
pal-1(zy117)
E
WT
N = 51
DA
DB
DD
Individual Worm
Neuron Position
pal-1(zy117)
N = 53
Neuron Position

FIG 2

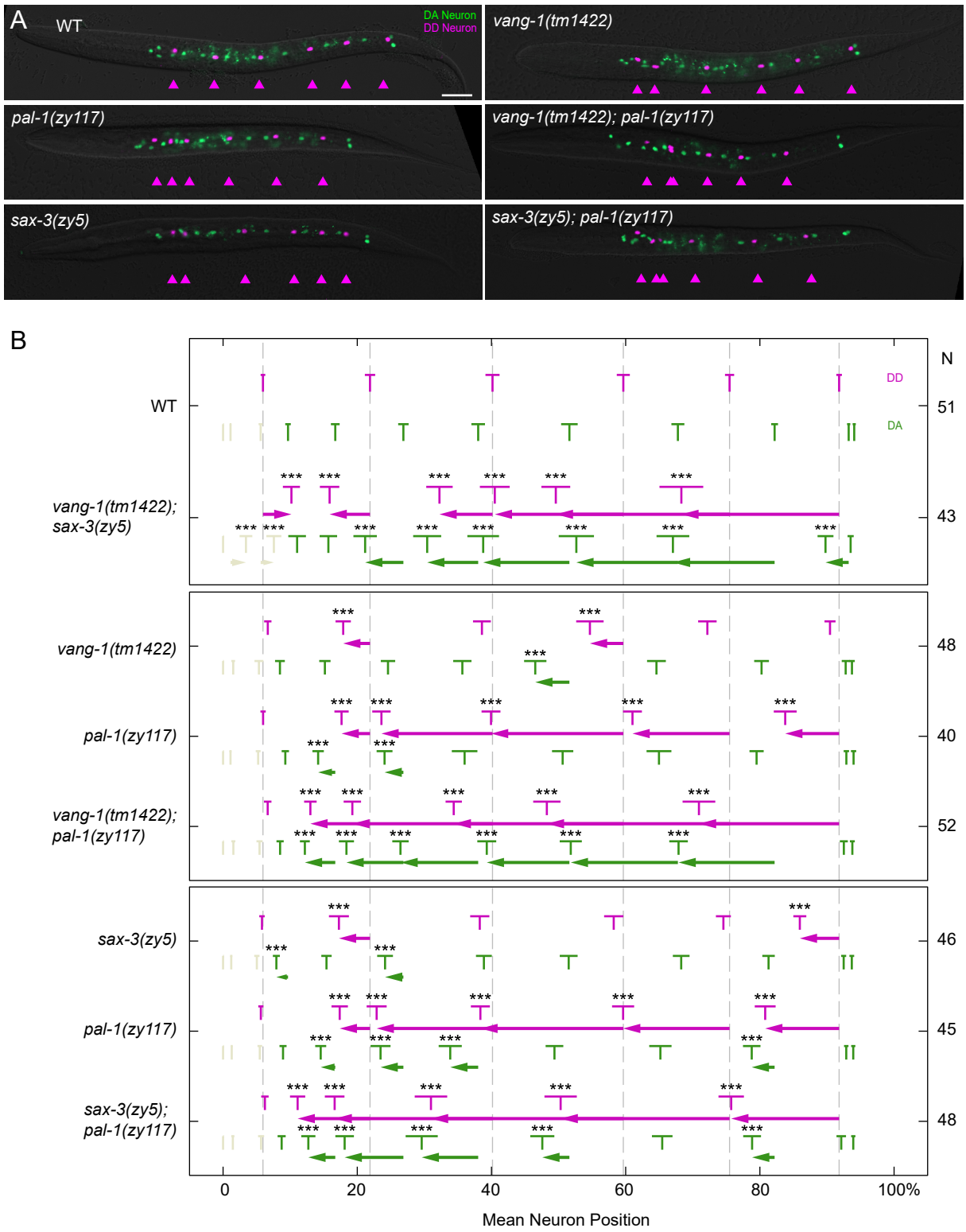
A
WT
DA Neuron
DD Neuron
vang-1(tm1422)
pal-1(zy117)
vang-1(tm1422); pal-1(zy117)
sax-3(zy5)
sax-3(zy5); pal-1(zy117)
B
N
DD
DA
WT
51
vang-1(tm1422);
sax-3(zy5)
43
vang-1(tm1422)
48
pal-1(zy117)
40
vang-1(tm1422);
pal-1(zy117)
52
sax-3(zy5)
46
pal-1(zy117)
45
sax-3(zy5);
pal-1(zy117)
48
0
20
40
60
80
100%
Mean Neuron Position

FIG 3

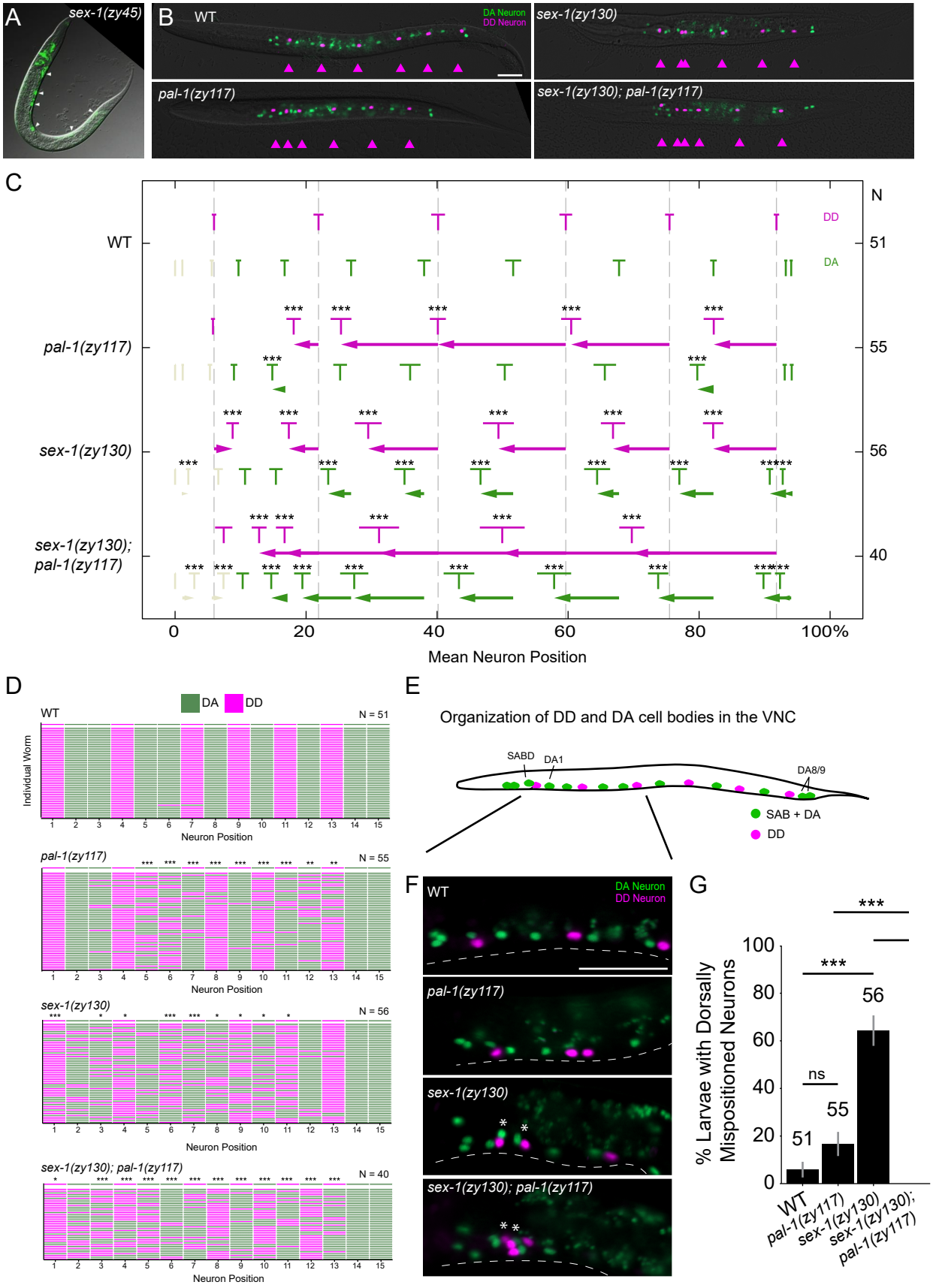
A
sex-1(zy45)
B
WT
DA Neuron
DD Neuron
sex-1(zy130)
pal-1(zy117)
sex-1(zy130); pal-1(zy117)
C
N
DD
DA
WT
51
pal-1(zy117)
55
sex-1(zy130)
56
sex-1(zy130);
pal-1(zy117)
40
0
20
40
60
80
100%
Mean Neuron Position
D
DA
DD
WT
N = 51
Individual Worm
Neuron Position
pal-1(zy117)
N = 55
sex-1(zy130)
N = 56
sex-1(zy130); pal-1(zy117)
N = 40
E
Organization of DD and DA cell bodies in the VNC
SABD
DA1
DA8/9
SAB + DA
DD
F
WT
DA Neuron
DD Neuron
pal-1(zy117)
sex-1(zy130)
sex-1(zy130); pal-1(zy117)
G
% Larvae with Dorsally Mispositioned Neurons
100
80
60
40
20
0
51
55
56
ns
WT
pal-1(zy117)
sex-1(zy130)
sex-1(zy130);
pal-1(zy117)

FIG 4

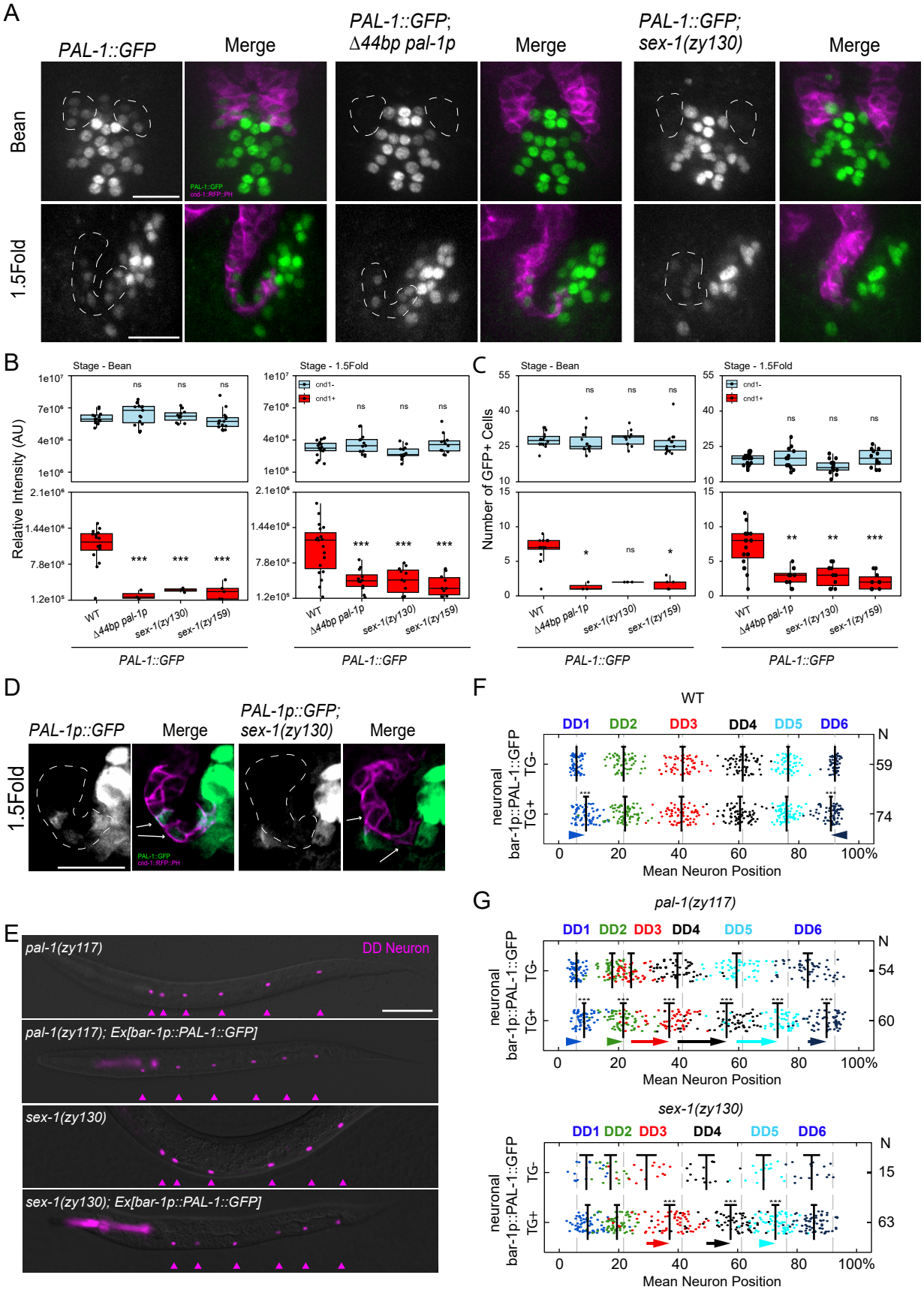
A
PAL-1::GFP
Merge
PAL-1::GFP; Δ44bp pal-1p
Merge
PAL-1::GFP; sex-1(zy130)
Merge
Bean
1.5Fold
B
Stage - Bean
Stage - 1.5Fold
Relative Intensity (AU)
cnd1-
cnd1+
ns
***
WT
Δ44bp pal-1p
sex-1(zy130)
sex-1(zy159)
PAL-1::GFP
C
Number of GFP+ Cells
D
PAL-1p::GFP
Merge
PAL-1p::GFP; sex-1(zy130)
Merge
1.5Fold
E
pal-1(zy117)
DD Neuron
pal-1(zy117); Ex[bar-1p::PAL-1::GFP]
sex-1(zy130)
sex-1(zy130); Ex[bar-1p::PAL-1::GFP]
F
WT
DD1 DD2 DD3 DD4 DD5 DD6
N
neuronal bar-1p::PAL-1::GFP
TG-
TG+
59
74
Mean Neuron Position
G
pal-1(zy117)
54
60
sex-1(zy130)
15
63

FIG 5